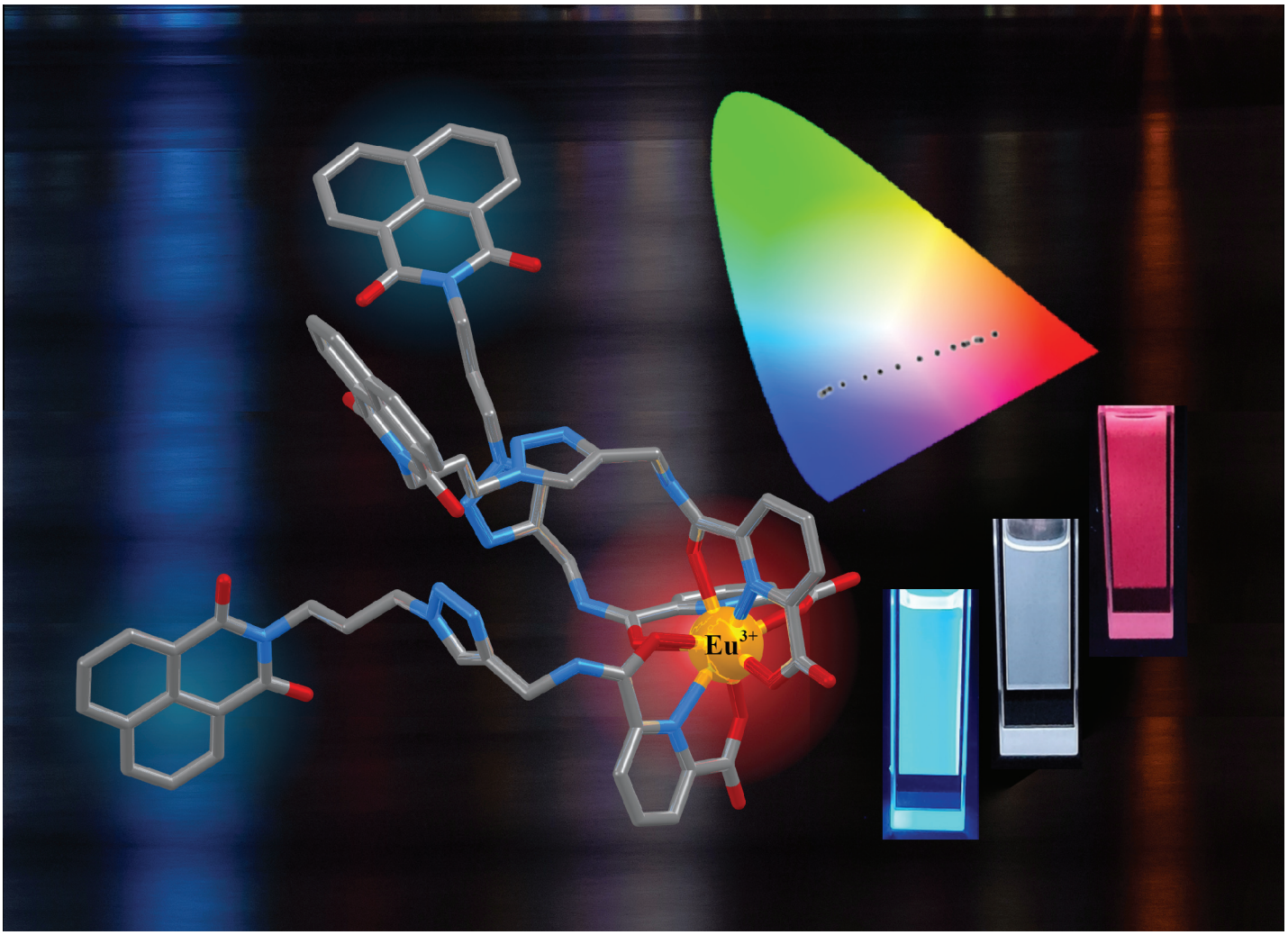

Showcasing research from Associate Professor Kitchen's laboratory, School of Natural Sciences, Massey University, Auckland, New Zealand.

White light and colour-tunable emission from a single component europium-1,8-naphthalimide thin film

In this contribution we describe the synthesis and fabrication of spin coated films of a new europium(III) complex derived from a 1,8-naphthalimide containing ligand. The complex is multi-emissive displaying blue emission from the 1,8-naphthalimide and red emission from the Eu^{3+} centre. Overall emission can be tuned by changing the excitation wavelength to give an overall emission colour from blue, to red and including white-light emission. The complex was spin-coated onto quartz slides giving coatings that retained the multi-emissive and colour tunable properties.

As featured in:

See Jonathan A. Kitchen *et al.*, *Dalton Trans.*, 2023, **52**, 2255.

ROYAL SOCIETY OF CHEMISTRY

rsc.li/dalton

Registered charity number: 207890

Dalton Transactions

ROYAL SOCIETY OF CHEMISTRY

PAPER

View Article Online
View Journal | View Issue

Cite this: *Dalton Trans.*, 2023, **52**, 2255

White light and colour-tunable emission from a single component europium-1,8-naphthalimide thin film†

Alex T. O'Neil, [a] Anaïs Chalard,[b,c] Jenny Malmström [b,c] and Jonathan A. Kitchen *[a,c]

Received 13th November 2022,
Accepted 1st December 2022

DOI: 10.1039/d2dt03644d

rsc.li/dalton

The synthesis and fabrication of spin coated films of a new Eu^{3+} complex [Eu(**1**)$_3$] derived from the 1,8-naphthalimide containing ligand **1H** is presented. The complex is multi-emissive displaying blue emission from the 1,8-naphthalimide fluorophore and red emission from the Eu^{3+} centre in both solution-state and solid-state. This allows the overall emission to be tuned by changing the excitaton wavelength, where varing degrees of red and blue emission intensity alter the overall emission colour from blue, to red and including white-light emission. The complex was spin-coated onto quartz slides giving 134 nm thick coatings that retained the multi-emissive and colour tunable properties. Overall, resulting in a colour-tunable system which in solution, solid, and thin film states can alter the overall colour from deep red to dark blue.

Introduction

Multi-emissive materials continue to attract significant attention from the chemistry research community. Their propensity towards advanced applications (ratiometric sensors,[1–3] molecular barcodes,[4] logic gates,[5] imaging agents,[6] and white emitting materials)[7–11] means they are high value targets. Various approaches to generating multi-emissive materials exist,[12–15] including the formation of supramolecular materials from trivalent lanthanide ions (Ln^{3+}).[7,11,16] Advantages of the supramolecular approach include combining both Ln^{3+} and ligand functionalities easily into a single component (*i.e.* a luminescent metal and a luminescent ligand to give multi-emission), inherently soluble systems that allow for solution processibility,[17] and modular design meaning the systems can be easily tuned or improved. Ln^{3+} are particularly attractive for the aforementioned applications owing to their excellent photophysical properties (long-lived excited states, solid-state emission, line-like emission bands and tunable quantum yields).[7,18] Whilst many multi-emissive Ln^{3+} containing systems are Metal Organic Frameworks (MOFs),[3] we are interested in discrete systems as these are typically more soluble and processable. Choice of ligand fluorophore plays an important role – it must be emissive in the correct wavelength range, easily tuned, and not reduce solubility. 1,8-Naphthalimides (**Nap**) are excellent candidates,[19] as they emit across a broad range of wavelengths,[20] their solubility is tunable, they are synthetically easy to include into ligands, and have proven layer forming abilities.[21–23] Naphthalimides have previously been used to generate Ln^{3+} complexes[21–30] including in white emissive lanthanide systems.[8,10] Ward and co-workers showed that single component multi-emission was possible by combining Eu^{3+} and **Nap** in a macrocyclic complex, achieving white emission in solution (CIE coordinates of x,y = 0.27, 0.25) and blue emission in thin films prepared by evaporation.[10] In comparison Yan and co-workers achieved white emission in the solid-state using Eu^{3+} and **Nap** carboxylate ligands (CIE coordinates x,y = 0.34, 0.31–pure white is considered x,y = 0.33).[8,10,31] However, to the best of our knowledge the naphthalimide–lanthanide combination has not been used to generate white-emissive *thin-films*. Herein, we report our approach to generating multi-emissive lanthanide thin-films by combining 1,8-naphthalimides and pyridine-2-carboxylate-6-amide (**PDC**) Ln^{3+} binding groups (Fig. 1). **PDC** is a relatively under-utilised motif for lanthanide assemblies but has both benefits of improved coordination of the more common dipicolinic acid (**DPA**) from the free carboxylate, and easy modification of the 2,6-pyridinedicarboxylate amide (**PDA**) through the amide side arm. **PDC** systems have shown to be effective sensitizers for a range of visibly emitting lanthanides.[32] With this in mind, we have utilised our previously developed 1,2,3-triazole "click" synthetic strategy[32–34] to functionalise **PDC** with a blue emissive **Nap** and complex with the visibly emissive lanthanide ion Eu^{3+}.

[a]*School of Natural Sciences, Massey University, Auckland, New Zealand. E-mail: j.kitchen@massey.ac.nz*
[b]*Department of Chemical and Materials Engineering, University of Auckland, Auckland 1142, New Zealand*
[c]*The MacDiarmid Institute for Advanced Materials and Nanotechnology, Wellington, New Zealand*

† Electronic supplementary information (ESI) available. See DOI: https://doi.org/10.1039/d2dt03644d

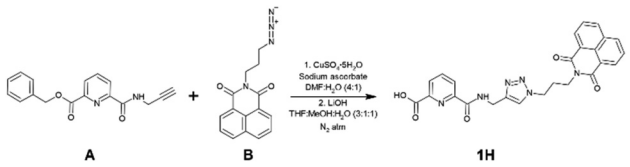

Fig. 1 Two stage synthesis of Ligand **1H** with CuACC "click" reaction between precursors **A** and **B** followed by deprotection of benzyl ester resulting in ligand **1H**.

Results and discussion

Ligand synthesis and characterisation

Ligand **1H** was synthesised in a converging seven-step synthesis starting from commercially available DPA and 1,8-naphthalic anhydride (Fig. 1).[32,33,35,36] 1,8-Naphthalic anhydride was converted into *N*-(3-azidopropyl)-1,8-naphthalimide (**B**) in a three step process following literature procedures[35,36] and then underwent a CuAAC reaction with our previously reported mono-alkyne (**A**)[32] at 80 °C in 4 : 1 DMF : H_2O forming the benzyl protected intermediate (**1Bz**).[32] Removal of the benzyl protecting group was carried out using LiOH following reported procedures[32] and resulted in **1H** as a off-white solid in 59% yield. All compounds were characterised using ^{1}H-NMR, ^{13}C-NMR, FTIR and Mass Spectrometry. Successful formation of **1H** was confirmed by LRMS with peaks at 485.10 *m*/*z* and 507.00 *m*/*z* corresponding to the [**1H** + H]$^+$ species (calc. for $C_{25}H_{21}N_6O_5^+$, 485.16) and [**1H** + Na]$^+$ species (calc. for $C_{25}H_{20}N_6O_5Na^+$, 507.14) respectively. ^{1}H-NMR also indicated successful formation of **1H**, particularly when comparing the spectra of **1H** with intermediate **1Bz** and precursors **A** and **B** (Fig. S21†). The appearance of a singlet resonance peak at ≈8.0 ppm assigned to the 1,2,3-triazole proton along with the corresponding disappearance of the terminal alkyne proton signal at 3.2 ppm of precursor **A** and downfield shifts observed in linking methylene groups bonded to the 1,2,3-triazole ring (t) (3.5 to 4.1 ppm for N_3–**CH_2** to t–**CH_2** and 4.2 to 4.6 ppm for NH–**CH_2**–**C** CH to NH–**CH_2**–t) post CuAAC reaction is evidence of successful 1,2,3-triazole formation in intermediate **1Bz**. Deprotection of the carboxylate, forming **1H**, is evident from the disappearance of the associated benzyl aromatic protons (Bz, 7.3–7.5 ppm) and the CH_2–Bz linker (5.4 ppm). ^{13}C NMR also confirmed formation of **1H** with the correct number of carbon environments and appearance of 1,2,3-triazole ring signals (144.8 (C) and 123.5 (CH) ppm).

Lanthanide complexation and characterisation

Ln(**1**)$_3$ complexes (Ln = Eu^{3+} and La^{3+}) were prepared by heating **1H** with 0.3 equivalents of $Ln(CF_3SO_3)\cdot xH_2O$ and 1 equivalent of NEt_3, in DCM : MeOH : $CHCl_3$ (3 : 3 : 2). Vapour diffusion of diethyl ether resulted in off-white solids in good yields (68–83%). Complexes were fully characterised by elemental analysis, FTIR, HRMS and ^{1}H-NMR (see ESI†). Lanthanide coordination within the **PDC** NO_2 pocket is suggested by the notable shift to lower energy for both the C=O stretches from 1739 cm^{-1} (carboxyl) and 1656 cm^{-1} (amide) to a merged peak at 1632 cm^{-1}, a shift commonly associated with coordination to Ln^{3+} ions (Fig. S22†).[37] While the carbonyl stretch associated with the **Nap** is seen to remain unchanged at 1693 cm^{-1}, indicating the lack of interaction between the Ln^{3+} and the **Nap** as expected. ^{1}H NMR of La(**1**)$_3$ (Fig. S28†) shows a significant downfield shift in the NH signal (0.71 ppm) and a corresponding upfield shift in the methylene linker (**CH_2**–NH, 0.18 ppm), previously observed in similar PDC systems and indicative of La^{3+} coordination in the NO_2 pocket.[38] While proton signals associated with the central pyridyl ring of the PDC motif (which overlapped as one signal in the **1H** spectrum) now separate into three distinct proton signals, while all other signals observed no significant shift, further indicative of lanthanide coordination occurring only within the **PDC** NO_2 pocket. HRMS (Fig. S24–S27†) showed ions with the expected masses and isotropic distributions: [Eu(**1**)$_3$ + 2Na]$^{2+}$ 824.1980 *m*/*z* (calc. for $C_{75}H_{57}N_{18}O_{15}EuNa_2$ 824.1630 *m*/*z*), and [La(**1**)$_3$ + 2Na]$^{2+}$ 817.1818 *m*/*z* (calc. for $C_{75}H_{57}N_{18}O_{15}LaNa_2$ 817.1549 *m*/*z*).

Photophysical properties

UV-visible absorption properties of **1H** and Ln(**1**)$_3$ complexes were measured in MeOH (Fig. S23†). **1H** showed a broad absorbance spectrum from 210 to 360 nm, significant absorptions are observed at 220 nm and 370 nm associated with n → π* and π → π* transitions from the **Nap**,[39] and weaker absorptions from 260–280 nm assigned to the n → π* and π → π* transitions from the central pyridyl unit.[33,40–42] Upon complexation the absorption spectra of all Ln^{3+} complexes underwent a slight red shift in the pyridyl associated bands while the **Nap** bands remained unshifted (Fig. S23†).

Photoluminescence studies of **1H** (Fig. S29†) showed the expected **Nap** monomer emission ranging from 350 to 450 nm, with λ_{max} = 388 nm in both the solution and solid states,[20] when excited into the **Nap** based absorption bands (240 or 340 nm). The fluorescence quantum yield in MeOH was 12.4%, similar to other 1,8-naphthalimide containing systems.[20,25,43]

Upon coordination, the **Nap** monomer emission at 388 nm was retained in all complexes (when excited at λ_{ex} = 240, 274 or 340 nm). However, an additional new broad peak at 490 nm was observed (Fig. 2 and S30–S31†). This is likely from the three **Nap** moieties being in close proximity within the complex, resulting in an excimer emission band – a known phenomenon in **Nap** systems.[20,44] Excitation spectra showed the excimer bands associated with the **Nap** motif.

Eu(**1**)$_3$ displayed strong Eu^{3+} centred emission (λ_{ex} between 210 and 290 nm) with (*J* = 0–4) transitions in both steady state and time delayed measurements, including the 581 nm $^5D_0 \rightarrow {}^7F_0$ transition indicative of an overall C_3 symmetry (Fig. S31 and 32†).[45] Emission lifetimes of the $^5D_0 \rightarrow {}^7F_2$ transition were found to be 1.175 ms and were best fit to a single exponential decay, indicative of a single species in solution (Fig. S33†). The overall quantum yield was determined to be 7.5% which is midrange for **PDC** based Eu^{3+} complexes.[32,38,46–48] Excitation

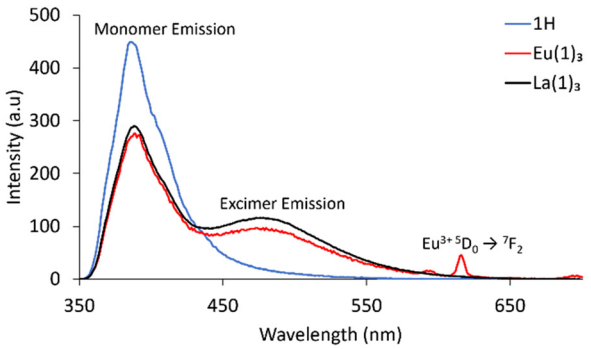

Fig. 2 Fluorescence spectra of **1H**, Eu(**1**)$_3$ and La(**1**)$_3$ showing excimer formation upon complexation (0.01 mM, MeOH, λ_{ex} = 300 nm).

plots indicated the primary antenna for Eu^{3+} centred emission is the pyridyl group with a major peak at 278 nm (Fig. S31†). Interestingly, there is a much smaller band from 300 to 350 nm associated with the **Nap** group, which can act as a secondary antenna. This is expected due to the **Nap** triplet state energy matching the Eu^{3+} excited state (18 500 cm^{-1} and 17 500 cm^{-1} respectively).[10]

Self-assembly studies

To further confirm that excimer formation was a result of complexation, concentration *vs.* emission intensity, and self-assembly studies of **1H** were carried out. At high concentrations of **1H** (10 mM) aggregation induced excimer emission was present. Upon reducing the concentration from 10 mM to 1 × 10^{-4} mM excimer emission disappeared with monomer emission becoming more intense (Fig. 3a). Fluorescence self-assembly studies between Eu^{3+} and **1H** (0.02 mM) showed that on addition of Eu^{3+} from 0 to 0.35 equiv. excimer (and Eu^{3+} centred) emission increased and monomer emission decreased. Excimer emission (and Eu^{3+} centred emission) peaked at 0.35 equivalents of Eu^{3+} while monomer emission reached a minimum, signifying the formation of the Eu(**1**)$_3$ complex and intramolecular interaction between neighbouring **Nap**, resulting in excimer emission (Fig. 3b and c).[44] Further addition of Eu^{3+} resulted in the formation of Eu(**1**)$_2$ and Eu(**1**) species (as seen in other **PDC** systems)[32] which was accompanied by decreased excimer emission and increased monomer emission, suggestive of all three **Nap** motifs situated on the same side of the Eu(**1**)$_3$ complex, thus maximising intramolecular interaction between neighbouring **Nap** (Fig. 3b and c).

Colour-tunability

With two well separated luminophores with different excitation wavelengths, the overall emission profile of Eu(**1**)$_3$ in solution (0.01 mM, MeOH) is dependent on the excitation wavelength (**Nap** emission at λ_{ex} = 200–240 nm and 290–350 nm, and Eu^{3+} emission at λ_{ex} = 245–290 nm, Fig. 4a, b and S39†). As a result, Eu(**1**)$_3$ is a rare example of a single component compound displaying colour-tunable emission. By simply altering the excitation wavelength, a large range of colour profiles were achieved. At excitation wavelengths below 240 nm blue emission was observed with **Nap**-based emission dominating the spectrum. Excitation at 245 nm resulted in increased Eu^{3+} emission and a colour-profile in the white emission region (CIE *x*,*y* = 0.35, 0.26). On increasing the excitation wavelength to 275 nm, where Eu^{3+} emission was maximised, bright red emission (CIE *x*,*y* = 0.54, 0.31) was observed. Further increasing the excitation to >290 nm, where Eu^{3+} emission reduced and **Nap** increased, gave the expected blue emission profile.

The colour-tunable emission can be further modified by changing the concentration to bring about aggregation-induced intermolecular excimer emission between complexes. Increasing the concentration from 0.01 mM to 1 mM, 5 mM and 10 mM significantly increased excimer emission (Fig. S40–42†). As a result, the colour-tunable window was reduced with the 1 mM solution only able to obtain a light red emission (Fig. S40†), and the 5 mM (Fig. S41†) and 10 mM (Fig. S42†) solutions unable to achieve red emission. The reduction of the colour-tunable window coincides with improved white emission where the 1 mM solution achieved close to pure-white emission when excited at 250 nm (CIE *x*,*y* = 0.33, 0.28). The 5 mM solution appeared white under short-wave UV irradiation (Fig. 4c) and achieved emission with CIE coordinates of *x*,*y* = 0.31, 0.27 when excited at 270 nm. A further increase to 10 mM caused overall emission to appear

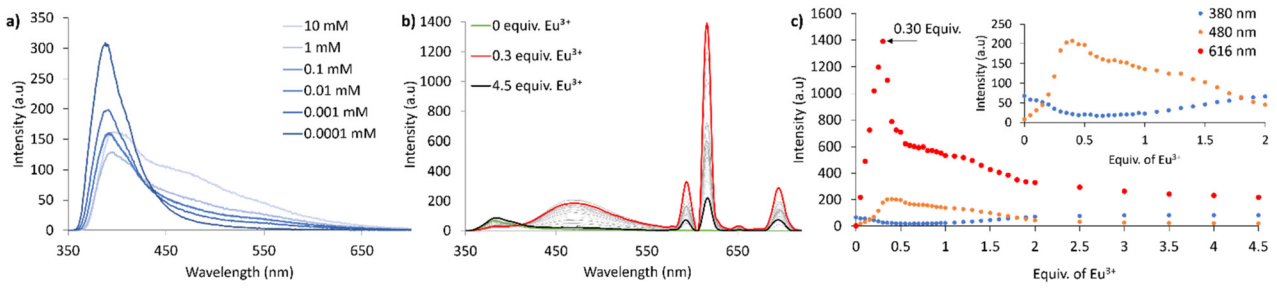

Fig. 3 (a) Fluorescence emission spectra (λ_{ex} = 340 nm) of **1H** at different concentrations showing aggregation induced excimer formation at higher concentrations in MeOH. (b) Fluorescence titration of **1H** with Eu(CF_3SO_3)$_3$ from 0 to 4.5 equivalents (λ_{ex} = 279 nm, 0.02 mM, MeOH). (c) Changes in fluorescence emission of **1H** (0.02 mM, MeOH) when titrated with Eu(CF_3SO_3)·6H_2O: **Nap** monomer emission at λ = 380 nm, **Nap** excimer emission at λ = 480 nm and Eu^{3+} emission at λ = 616 nm.

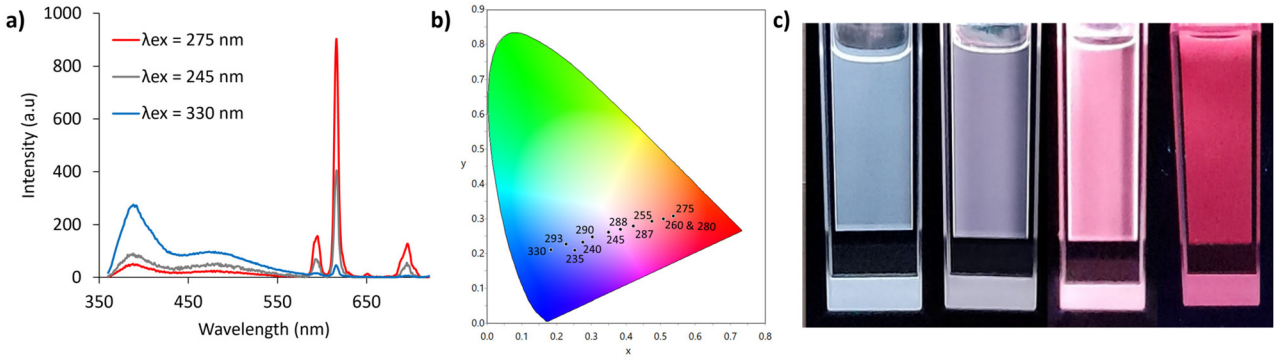

Fig. 4 (a) Eu(**1**)$_3$ fluorescent emission (0.01 mM, MeOH), showing Eu^{3+} centred emission *vs.* **Nap** centred emission at critical wavelengths. (b) CIE chromaticity diagram showing the colour-tunable emission range of Eu(**1**)$_3$ in solution (0.01 mM, MeOH). (c) Different concentrations of Eu(**1**)$_3$ in MeOH ranging from 10, 5, 1, 0.01 mM left to right, under shortwave UV light (λ_{ex} = 254 nm).

blue-white under shortwave UV (Fig. 4c) and excitation at 270 nm gave white emission (CIE x,y = 0.28, 0.26) similar to Ward and co-workers system.[10]

Solid state emission properties

The colour-tunable emission was also observed in the solid state. As expected, with only a **Nap** luminophore, solids of **1H** and La(**1**)$_3$ gave bright blue emission under both shortwave (λ_{ex} = 254 nm) and longwave (λ_{ex} = 365 nm) irradiation. While Eu(**1**)$_3$ displayed colour-tunable emission (Fig. 5), switching from bright blue to white under long- and short-wave UV respectively. Solid state fluorescence showed increased excimer emission, and a colour-tunable window similar to that observed in the Eu(**1**)$_3$ 5 mM solution (Fig. S41†). Excitation outside of the 260–288 nm range resulted in overall blue emission while between these excitation wavelengths, overall emission was white with CIE coordinates ranging within x = 0.28–0.32 and y = 0.29. Nearest to pure white was achieved when λ_{ex} = 275 nm with CIE coordinates x,y = 0.32, 0.29.

Thin film fabrication

With Eu(**1**)$_3$ displaying colour-tunable and white emission observed in both solid- and solution-states we next investigated the ability of Eu(**1**)$_3$ to form thin films through spin coating deposition. A 10 mg ml^{-1} solution of Eu(**1**)$_3$ in DCM : MeOH : DMF (4 : 4 : 2) was spin coated onto 15 × 20 mm glass and 20 × 20 mm quartz substrates. 50 μL was dynamically deposited onto the substrates at 500 rpm and then spun up to 4000 rpm, resulting in a uniform film to the eye (Fig. 6). AFM measurements showed a stippled coating with an average particle height of 133.5 nm, while also containing some larger aggregates (see Fig. S45 and 46†). Importantly, the film retained the properties exhibited in the solution and bulk solid states. The film appeared bright white under short-wave and light blue under long-wave UV irradiation (Fig. 6). Photophysical measurements were carried out on the film showing that it retained the same absorption profile of Eu(**1**)$_3$ as measured in solution (Fig. S44†). Fluorescence emission showed a similar colour-tunable emission profile to the solid state (and high concentration solution) with strong excimer emission (Fig. S47†). Excitation wavelengths outside of the 260–288 nm range resulted in overall blue emission as it favours **Nap** excimer emission. Excitation between 260–288 nm (where Eu^{3+} centred emission increases) resulted in overall emission within the white region with CIE coordinates ranging within x = 0.28–0.34 and y = 0.26–0.28 (Fig. 6). Closest to pure white emission is achieved over a range of excitation wavelengths (λ_{ex} = 270–272, 279–283 nm) with CIE coordinates

Fig. 5 Eu(**1**)$_3$ solid powder, shown (left to right) under ambient light, 254 nm UV irradiation and 365 nm UV irradiation.

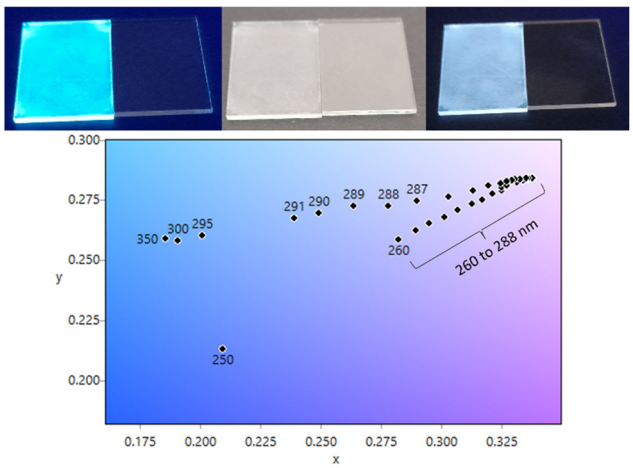

Fig. 6 (Top) Spin coated films of Eu(**1**)$_3$ on a 15 × 20 mm glass substrate, under 365 nm, ambient light and 254 nm UV irradiation, respectively. (Bottom) CIE coordinates showing the colour-tunable emission range for the Eu(**1**)$_3$ spin coated film (see ESI† for CIE coordinates).

equalling x,y = 0.33, 0.28, close to the emission of the original solid. While λ_{ex} of 273–278 nm emission is still close to pure white with CIE coordinates x,y = 0.34, 0.28.

Conclusions

The discrete lanthanide complex Eu(**1**)$_3$ resulted in the formation of a multi-emissive assembly capable of colour-tunable emission dependent on the excitation wavelength ranging from blue to red and close to white emission in solution and solid states. With Eu(**1**)$_3$ being a discrete system, it is easily solubilised in a range of solvents. This allowed Eu(**1**)$_3$ to form thin films by spin coating. The thin films retained both colour-tunability and white emission, which to the best of our knowledge is the first example of a discrete Ln^{3+}-1,8-naphthalimide complex processed into thin films that exhibit such properties. Additionally, the luminophores were observed to act almost independently from each other at most excitation wavelengths. Such multi-emission is ideal for sensor development, as it allows for self-calibrating ratiometric systems.[1,49,50] We are currently investigating the potential for self-calibrating ratiometric oxygen sensors both in solution and as films, in which the organic emission is quenched in the presence of oxygen, while the Ln^{3+} signal self-calibrates and regulates signal change.

Experimental

General experimental details

All reagents, solvents and starting materials were purchased from Sigma-Aldrich. Precursors **A**[32] and **B**[35,36] were synthesised using literature methods and showed the expected characterisation. NMR spectra were recorded using a Bruker Ultrashield 300, with chemical shifts recorded in parts per million (ppm) downfield from the standard. UV-visible absorption was recorded on a Shimadzu UV-1800 using CH_2Cl_2 and MeOH solvents in a 3 mL quartz cuvette with a 1 cm path length. Steady state–fluorescence measurements were recorded on a Shimadzu RF-6000 Spectro fluorophotometer and time resolved phosphorescence measurements were carried out using an Agilent Technologies Cary Eclipse fluorescence spectrophotometer, with CH_2Cl_3 and MeOH solvents in a capped 3.5 mL quartz cuvette with a 1 cm path length. *Self-assembly titrations*: The formation of 1 : 1, 1 : 2 and 1 : 3 (M : L) species was monitored by measuring changes in the UV-visible absorption and fluorescence spectra (λ_{ex} = 279 nm) of **1H** (2×10^{-5} M in 3 mL volume in MeOH diluted from 0.001 M stock solution in DCM : MeOH (1 : 1)) when titrated with Eu$(CF_3SO_3)_3{\cdot}6H_2O$ solution (1 mM, MeOH) from 0→4.5 equivalents, with 3 μL additions for 0 to 1 equivalents, 6 μL additions for 1 to 2 equivalents, and 30 μL additions for 2 to 4.5 equivalents. Commission Internationale de l'Eclairage (CIE) plots were generated in OSRAM LED ColorCalculator software. Melting points were obtained on a Electrothermal IA9000 Series Melting Point Apparatus. Fourier-transform infrared spectroscopy (FTIR) of solids were recorded on a Bruker Alpha platinum-ATR. Mass spectrometry of ligands was carried out in HPLC grade solvents, on a Shimadzu LCMS-2020 for ligands and a Bruker Daltonics MicrOTOF™ Spectrometer for complexes. Spin coated films were fabricated on an Ossila spin coater using 1 mm thick quartz substrates (10 mm × 15 mm). Atomic force microscopy (AFM) measurements were performed in tapping mode, on an Asylum Cypher ES (Oxford Instruments, US). AFM tip parameters with silicon probes (nominal spring constant 5 N m^{-1}, resonance frequency 150 kHz, from Budget Sensors, Bulgaria), with a set point at 80% amplitude and measurements run in attractive mode. Safety Note: whilst no issues were encountered here, low molecular weight organic azides are potential explosives and care must be taken during their handling.

Quantum yield measurements

Quantum yield measurements were determined by the dilute comparison method[51] using relative standards Cs_3[Eu$(dpa)_3$]·$8H_2O$,[52,53] complex in a 0.1 M tris-HCl buffer solution (pH ≈ 7.45) and quinine sulfate in 0.5 M H_2SO_4,[54] with known quantum yields of Φ_{ref} = 24 ± 2.5%, and Φ_{ref} = 54.6% respectively. Cs_3[Eu$(dpa)_3$]·$9H_2O$ was used for Eu(**1**)$_3$ and quinine sulfate was used for the 1,8-naphthalimide emission. Barrier slit widths remained the same between measurements for different compounds with 1.5, 3 nm excitation and emission widths. Excitation wavelength was the same for all measurements with the standard 279 nm excitation wavelength being used for Eu^{3+} emissions and 366 nm for quinine sulfate and **Nap** emissions. Complexes were dissolved in a 1 : 1 MeOH : CH_2Cl_2 and then diluted into MeOH.

$$\Phi_x = \Phi_{std}\left(\frac{grad_x}{grad_{ref}} \times \left(\frac{{n_x}^2}{{n_{ref}}^2}\right)\right) \quad (1)$$

Estimated overall quantum yields $\Phi^L_{Ln} = \Phi_x$ were calculated according to eqn (1).[51,52] Here grad refers to the slope of plotted emission area *vs.* absorbance (emission area was taken from specific emission peaks, Eu(**1**)$_3$ ($^5D_0 \rightarrow {}^7F_2$), and 1,8-naphthalimide excimer and monomer broad emissions *vs.* quinine sulfate), n refers to refractive index of the solution (a refractive index of n = 1.3295 was found for MeOH : CH_2Cl_2 solution), and subscripts are ref for reference and x for sample.[51,52]

Synthesis of N_2-bis((1-(*N*-(3-propyl)-1,8-naphthalimide)-1*H*-1,2,3-triazol-4-yl)methyl)-O_6-((benzyloxy)carbonyl)pyridine-2 carboxamide-6-carboxylate (1Bz)

A (0.400 g, 1.4 mM) was combined with sodium ascorbate (0.269 g, 1.4 mM), $CuSO_4{\cdot}5H_2O$ (0.170 g, 0.7 mM) and **B** (0.381 g, 1.4 mM) in 30 mL of DMF : H_2O (4 : 1). The solution was heated to 80 °C overnight, changing from a light yellow to a dark green. Water was slowly added to the solution until a cloudy precipitate formed, which was filtered and then washed with 0.1 M NaOH/0.5 M EDTA solution yielding **1Bz** as an off-

white solid (0.558 g, 71%). Melting point = 143.3 °C. LRMS *m*/*z* = 575.15 [**1Bz** + H]$^+$ (calc. for $C_{32}H_{27}N_6O_5^+$, 575.20). ^{1}H NMR (300 MHz, DMSO-d$_6$, ppm), δ = 9.04 (t, *J* = 6.0 Hz, 1H, NH), 8.49 (t, *J* = 7.0, 4H, Nap–H), 8.27 (m, 3H, Py–H), 8.05 (s, 1H, t–H), 7.89 (m, 2H, Nap–H), 7.41 (m, 5H, Bz–H), 5.45 (s, 1H, **CH$_2$**–Bz), 4.59 (d, *J* = 5.5 Hz, 2H, NH–**CH$_2$**–t), 4.48 (t, *J* = 7.0 Hz, 2H, t–**CH$_2$**), 4.15 (t, *J* = 7.0 Hz, 2H, CH$_2$–Nap), 2.23 (m, 2.23, CH$_2$–**CH$_2$**–CH$_2$); ^{13}C NMR (75 MHz, DMSO-d$_6$, ppm): δ = 164.3 (C═O–Py), 164.1 (C═O–Nap), 163.6 (C═O–Py), 150.6 (CN–Py), 146.9 (CN–Py), 144.8 (C–t), 140.0 (CH–Py), 136.2 (C–Bz), 134.7 (CH–Nap), 131.7 (C–Nap), 131.1 (CH–Nap), 129.0 (CH–Bz), 128.7 (CH–Bz), 128.5 (CH–Bz), 127.9 (C–Nap), 127.9 (CH–Py), 127.6 (CH–Nap), 125.9 (CH–Py), 123.5 (CH–t), 122.6 (C–Nap), 67.3 (CH$_2$–Bn), 48.0 (CH$_2$), 37.8 (CH$_2$), 35.2 (CH$_2$–NH), 29.0 (CH$_2$). FTIR (cm^{-1}) 1779, 1734, 1695, 1651, 1585, 1531, 1438, 1348, 1305, 1305, 1232, 1171, 1124, 1049, 1002, 907, 843, 773, 745, 675, 643, 541, 514.

Synthesis of N_2-((1-(*N*-(3-propyl)-1,8-naphthalimide)-1*H*-1,2,3-triazol-4-yl)methyl)pyridine-2-carboxamide-6-carboxylate (1H)

1Bz (0.858 g, 1.5 mM) was combined with LiOH (0.143 g, 6.0 mM) in 20 mL of THF : MeOH : H$_2$O (3 : 1 : 1). This was stirred overnight under a nitrogen atmosphere, where the solid slowly dissolved into a light-yellow solution. The solvent was then removed resulting in an oily residue. 1 M HCl was then added causing an off-white precipitate to form, which was filtered and washed with water and acetone to remove the 1,8-naphthalimide by-product, yielding **1H** as an off-white solid (0.428 g, 59%). Melting point = 148.2 °C. LRMS *m*/*z* = 485.10 [**1H** + H]$^+$ (calc. for $C_{25}H_{21}N_6O_5^+$, 485.16) and *m*/z = 507.00 [**1H** + Na]$^+$ (calc. for $C_{25}H_{20}N_6O_5Na^+$, 507.14). ^{1}H NMR (300 MHz, DMSO-d$_6$, ppm), δ = 9.71 (t, *J* = 6.0 Hz, 1H, NH), 8.46 (t, *J* = 6.0, 4H, Nap–H), 8.23 (m, 3H, Py–H), 8.05 (s, 1H, t–H), 7.87 (m, 2H, Nap–H), 4.58 (d, *J* = 6.0 Hz, 2H, NH–**CH$_2$**–t), 4.45 (t, *J* = 7.0 Hz, 2H, t–CH$_2$), 4.11 (t, *J* = 7.0 Hz, 2H, CH$_2$–Nap), 2.20 (m, 2H, CH$_2$–**CH$_2$**–CH$_2$); ^{13}C NMR (75 MHz, DMSO-d$_6$, ppm): 165.4 (C═O–Py), 164.1 (C═O–Nap), 163.3 (C═O–Py), 149.5 (CN–Py), 146.4 (CN–Py), 144.8 (C–t), 140.4 (CH–Py), 134.8 (CH–Nap), 131.8 (C–Nap), 131.2 (CH–Nap), 127.9 (C–Nap), 127.7 (CH–Nap), 127.1 (CH–Py), 125.9 (CH–Py), 123.6 (CH–t), 122.8 (C–Nap), 48.0 (CH$_2$), 37.8 (CH$_2$), 34.9 (CH$_2$–NH), 29.0 (CH$_2$). FTIR (cm^{-1}) 3234, 3138, 2925, 2853, 2394, 1893, 1739 (COOH–Py), 1695 (CO–Nap), 1657 (CONH–Py), 1625, 1587, 1530, 1454, 1440, 1387, 1345, 1306, 1235, 1170, 1147, 1121, 1074, 1054, 1016, 1001, 963, 907, 880, 847, 801, 780, 765, 747, 682, 643, 628, 563, 546, 516, 489, 423.

Synthesis of Eu(1)$_3$

1H (0.0640 g, 0.132 mM) was combined with Eu(CF$_3$SO$_3$)$_3$·6H$_2$O (0.0308 g, 0.044 mM) and 1 equivalent of triethylamine in 5 mL of DCM : MeOH : CHCl$_3$ (3 : 3 : 2). The complex precipitated as a white powder, which was filtered giving Eu(**1**)$_3$ as a white solid (0.058 g, 83%). Melting point = 205–226 °C. HRMS *m*/*z* = 824.1980 [Eu(**1**)$_3$ + 2Na]$^{2+}$ (calc. for $(C_{75}H_{57}N_{18}O_{15}EuNa_2)^{2+}$, 824.1630), *m*/*z* = 1625.3545 [Eu(**1**)$_3$ + Na]$^+$ (calc. for $(C_{75}H_{57}N_{18}O_{15}EuNa)^+$, 1625.3367). FTIR (cm^{-1}) 3233, 3073, 2965, 1698, 1633, 1587, 1565, 1462, 1430, 1347, 1277, 1235, 1155, 1082, 1048, 1029, 1018, 890, 848, 801, 779, 761, 724, 687, 660, 637, 573, 540, 517, 410. Elemental analysis for $C_{75}H_{57}N_{18}O_{15}Eu{\cdot}3.5H_2O{\cdot}2.5CH_2Cl_2$ (1878.7389 g mol^{-1}) calculated: C 49.55, H 3.70, N 13.42%. Found C 49.74, H 4.00, N 13.45%.

Synthesis of La(1)$_3$

1H (0.0622 g, 0.128 mM) was combined with La(CF$_3$SO$_3$)$_3$·9H$_2$O (0.0317 g, 0.044 mM) and 1 equivalent of triethylamine in 5 mL of DCM : MeOH : CHCl$_3$ (3 : 3 : 2). The complex precipitated as a white powder, which was filtered giving La(**1**)$_3$ as a white solid (0.046 g, 68%). HRMS *m*/*z* = 817.1818 [La(1)$_3$ + 2Na]$^{2+}$ (calc. for $(C_{75}H_{57}N_{18}O_{15}LaNa_2)^{2+}$, 817.1549). FTIR (cm^{-1}) 3270, 3080, 2967, 2337, 2318, 1697, 1624, 1587, 1566, 1436, 1347, 1275, 1235, 1169, 1084, 1049, 1030, 890, 847, 801, 778, 759, 723, 687, 637, 573, 540, 516, 407. Elemental analysis for $C_{75}H_{57}N_{18}O_{15}La{\cdot}2{\cdot}CHCl_3$ (1860.0489 g mol^{-1}) calculated: C 49.72, H 3.20, N 13.55%. Found C 49.76, H 3.46, N 13.37%. ^{1}H NMR (300 MHz, DMSO-d$_6$, ppm), δ = 10.43 (t, *J* = 6.0 Hz, 1H, NH), 8.45 (t, *J* = 6.0, 4H, Nap–H), 8.37 (m, 1H, Py–H), 8.22 (m, 1H, Py–H), 8.1 (s, 1H, t–H), 7.91 (m, 1H, Py–H), 7.83 (m, 2H, Nap–H), 4.48 (d, *J* = 6.0 Hz, 2H, CH$_2$–Nap), 4.40 (t, *J* = 7.0 Hz, 2H, NH–**CH$_2$**–t), 4.11 (t, *J* = 7.0 Hz, 2H, t–**CH$_2$**), 2.20 (m, 2H, CH$_2$–**CH$_2$**–CH$_2$).

Author contributions

Alex O'Neil: conceptualisation, investigation, methodology, analysis, writing – original draft. Anaïs Chalard: AFM investigation, writing – review & editing. Jenny Malmström: supervision, AFM investigation, writing – review & editing. Jonathan Kitchen: conceptualisation, writing – review & editing, supervision, project administration.

Conflicts of interest

There are no conflicts to declare.

References

1 Y. Feng, J. Cheng, L. Zhou, X. Zhou and H. Xiang, *Analyst*, 2012, **137**, 4885–4901.
2 Y. Zhou and B. Yan, *J. Mater. Chem.*, 2015, **3**, 9353–9358.
3 T. Sun, Y. Gao, Y. Du, L. Zhou and X. Chen, *Front. Chem.*, 2021, **8**, 624592.
4 J. Wang, Y. Suffren, C. Daiguebonne, S. Freslon, K. Bernot, G. Calvez, L. Le Pollès, C. Roiland and O. Guillou, *Inorg. Chem.*, 2019, **58**, 2659–2668.
5 M. A. Hernández-Rodríguez, C. D. S. Brites, G. Antorrena, R. Piñol, R. Cases, L. Pérez-García, M. Rodrigues, J. A. Plaza, N. Torras, I. Díez, A. Millán and L. D. Carlos, *Adv. Opt. Mater.*, 2020, **8**, 2000312.

6 D. Kim, K. Jeong, J. E. Kwon, H. Park, S. Lee, S. Kim and S. Y. Park, *Nat. Commun.*, 2019, **10**, 3089.
7 S. SeethaLekshmi, A. R. Ramya, M. L. P. Reddy and S. Varughese, *J. Photochem. Photobiol., C*, 2017, **33**, 109–131.
8 J. Zhang, H. Li, P. Chen, W. Sun, T. Gao and P. Yan, *J. Mater. Chem. C*, 2015, **3**, 1799–1806.
9 O. Kotova, S. Comby, C. Lincheneau and T. Gunnlaugsson, *Chem. Sci.*, 2017, **8**, 3419–3426.
10 A. H. Shelton, I. V. Sazanovich, J. A. Weinstein and M. D. Ward, *Chem. Commun.*, 2012, **48**, 2749–2751.
11 R. Boddula, J. Tagare, K. Singh and S. Vaidyanathan, *Mater. Chem. Front.*, 2021, **5**, 3159–3175.
12 V. Anand, R. Mishra and Y. Barot, *Dyes Pigm.*, 2021, **191**, 109390.
13 N.-C. Chiu, K. T. Smith and K. C. Stylianou, *Coord. Chem. Rev.*, 2022, **459**, 214441.
14 N. Kim, J. Jeong and H. Chae, *Appl. Sci. Converg. Technol.*, 2016, **25**, 1–6.
15 P. Coppo, M. Duati, V. N. Kozhevnikov, J. W. Hofstraat and L. De Cola, *Angew. Chem., Int. Ed.*, 2005, **44**, 1806–1810.
16 A. R. Ramya, S. Varughese and M. L. P. Reddy, *Dalton Trans.*, 2014, **43**, 10940–10946.
17 J.-H. Jou, S. Sahoo, D. K. Dubey, R. A. K. Yadav, S. S. Swayamprabha and S. D. Chavhan, *J. Mater. Chem.*, 2018, **6**, 11492–11518.
18 J.-C. G. Bünzli and C. Piguet, *Chem. Soc. Rev.*, 2005, **34**, 1048–1077.
19 P. Gopikrishna, N. Meher and P. K. Iyer, *ACS Appl. Mater. Interfaces*, 2018, **10**, 12081–12111.
20 D. W. Cho and D. W. Cho, *New J. Chem.*, 2014, **38**, 2233–2236.
21 A. B. Carter, N. Zhang, I. A. Kühne, T. D. Keene, A. K. Powell and J. A. Kitchen, *ChemistrySelect*, 2019, **4**, 1850–1856.
22 D. L. Reger, A. P. Leitner and M. D. Smith, *Cryst. Growth Des.*, 2016, **16**, 527–536.
23 D. L. Reger, A. Leitner and M. D. Smith, *Cryst. Growth Des.*, 2015, **15**, 5637–5644.
24 K. R. Johnson and A. de Bettencourt-Dias, *Inorg. Chem.*, 2019, **58**, 13471–13480.
25 Z. Wang, N. Liu, H. Li, P. Chen and P. Yan, *Eur. J. Inorg. Chem.*, 2017, **2017**, 2211–2219.
26 V. F. Plyusnin, A. S. Kupryakov, V. P. Grivin, A. H. Shelton, I. V. Sazanovich, A. J. H. M. Meijer, J. A. Weinstein and M. D. Ward, *Photochem. Photobiol. Sci.*, 2013, **12**, 1666–1679.
27 C. S. Bonnet, M. Devocelle and T. Gunnlaugsson, *Org. Biomol. Chem.*, 2012, **10**, 126–133.
28 M. A. Alcala, C. M. Shade, H. Uh, S. Y. Kwan, M. Bischof, Z. P. Thompson, K. A. Gogick, A. R. Meier, T. G. Strein, D. L. Bartlett, R. A. Modzelewski, Y. J. Lee, S. Petoud and C. K. Brown, *Biomaterials*, 2011, **32**, 9343–9352.
29 J. Tang, H. Yang, J. Liu, Y. Wang, X. Yin, R. Wang, L. Huang and Z. Huang, *Opt. Mater.*, 2010, **32**, 1417–1422.
30 J. E. Elbert, S. Paulsen, L. Robinson, S. Elzey and K. Klein, *J. Photochem. Photobiol., A*, 2005, **169**, 9–19.
31 S. Dang, J.-H. Zhang and Z.-M. Sun, *J. Mater. Chem.*, 2012, **22**, 8868–8873.
32 A. T. O'Neil, J. A. Harrison and J. A. Kitchen, *Chem. Commun.*, 2021, **57**, 8067–8070.
33 A. T. O'Neil, N. Zhang, J. A. Harrison, S. M. Goldup and J. A. Kitchen, *Supramol. Chem.*, 2021, **33**, 160–173.
34 A. T. O'Neil and J. A. Kitchen, *Chemistry*, 2022, **4**, 1457–1465.
35 U. H. Sk and S. Bhattacharya, *Environ. Toxicol. Pharmacol.*, 2006, **22**, 298–308.
36 Q. M. Chen, Z. Li, G. X. Tian, Y. Chen and X. H. Wu, *J. Chem. Res.*, 2020, **45**, 258–264.
37 R. Jagannathan and S. Soundararajan, *J. Coord. Chem.*, 1979, **9**, 31–35.
38 O. Kotova, S. Blasco, B. Twamley, J. O'Brien, R. D. Peacock, J. A. Kitchen, M. Martínez-Calvo and T. Gunnlaugsson, *Chem. Sci.*, 2015, **6**, 457–471.
39 J. Gawronski, K. Gawronska, P. Skowronek and A. Holmén, *J. Org. Chem.*, 1999, **64**, 234–241.
40 T. Le Borgne, J.-M. Bénech, S. Floquet, G. Bernardinelli, C. Aliprandini, P. Bettens and C. Piguet, *Dalton Trans.*, 2003, 3856–3868.
41 F. Renaud, C. Piguet, G. Bernardinelli, J.-C. G. Bünzli and G. Hopfgartner, *Chem. – Eur. J.*, 1997, **3**, 1646–1659.
42 A.-S. Chauvin, J.-C. G. Bünzli, F. Bochud, R. Scopelliti and P. Froidevaux, *Chem. – Eur. J.*, 2006, **12**, 6852–6864.
43 V. F. Plyusnin, A. S. Kupryakov, V. P. Grivin, A. H. Shelton, I. V. Sazanovich, A. J. Meijer, J. A. Weinstein and M. D. Ward, *Photochem. Photobiol. Sci.*, 2013, **12**, 1666–1679.
44 M. Licchelli, A. O. Biroli, A. Poggi, D. Sacchi, C. Sangermani and M. Zema, *Dalton Trans.*, 2003, 4537–4545.
45 K. Binnemans, *Coord. Chem. Rev.*, 2015, **295**, 1–45.
46 J.-M. Senegas, G. Bernardinelli, D. Imbert, J.-C. G. Bünzli, P.-Y. Morgantini, J. Weber and C. Piguet, *Inorg. Chem.*, 2003, **42**, 4680–4695.
47 B.-L. An, M.-L. Gong, J.-M. Zhang and S.-L. Zheng, *Polyhedron*, 2003, **22**, 2719–2724.
48 B.-L. An, M.-L. Gong, K.-W. Cheah, J.-M. Zhang and K.-F. Li, *Chem. Phys. Lett.*, 2004, **385**, 345–350.
49 A. P. Demchenko, *Lab Chip*, 2005, **5**, 1210–1223.
50 M. Amelia, A. Lavie-Cambot, N. D. McClenaghan and A. Credi, *Chem. Commun.*, 2011, **47**, 325–327.
51 G. A. Crosby and J. N. Demas, *J. Phys. Chem.*, 1971, **75**, 991–1024.
52 A. S. Chauvin, F. Gumy, D. Imbert and J. C. G. Bünzli, *Spectrosc. Lett.*, 2004, **37**, 517–532.
53 A. S. Chauvin, F. Gumy, D. Imbert and J. C. G. Bünzli, *Spectrosc. Lett.*, 2007, **40**, 193–193.
54 A. M. Brouwer, *Pure Appl. Chem.*, 2011, **83**, 2213–2228.